Electronic Supplementary Material (ESI) for Chemical Communications.

Supplementary Information

A circulating electrolyte for a high performance carbon-based dye-sensitized solar cell†

Shuai Gu,[‡a] Enbing Bi,[‡b] Bitian Fu,[c] Gjergj Dodbiba,[a] Toyohisa Fujita,[a] David P. Wilkinson, [*d] Yuezhou Wei[*e] and Baizeng Fang[*d]

‡ These authors contributed equally.

[a] Graduate School of Engineering, The University of Tokyo, 113-8656, Japan.

[b] State Key Laboratory of Metal Matrix Composites, School of Materials Science and Engineering, Shanghai Jiao Tong University, Shanghai 200240, China.

[c] School of Ecological and Environmental Science, East China Normal University, Shanghai 200241, China

[d] Department of Chemical & Biological Engineering, University of British Columbia, 2360 East Mall, Vancouver, B.C., V6T 1Z3, Canada. Email: dwilkinson@chbe.ubc.ca (D. W.) bfang@chbe.ubc.ca (B. F.)

[e] College of Resources and Metallurgy, Guangxi University, Nanning 530004, Guangxi, China. Email: yzwei@gxu.edu.cn

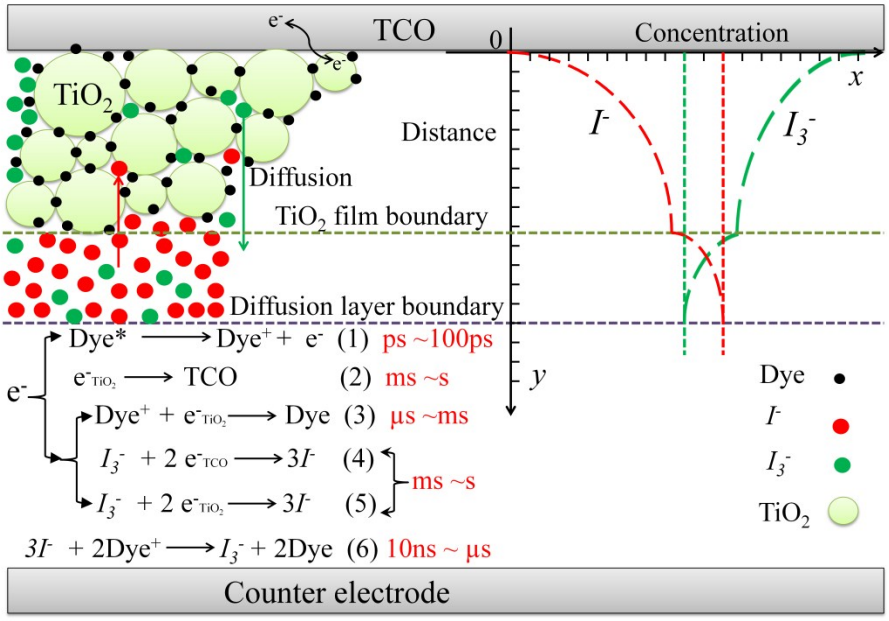

Figure S1. Schematic DSC configuration and the concentration distribution of I^- and I_3^- ions in the DSC. Black solid circles stand for the dyes adsorbed onto TiO_2 nanocrystalline, red solid circles stand for I^- ions, green solid circles stand for I_3^- ions, and olive solid circles stand for TiO_2 nanocrystalline. The olive dotted line demonstrates the boundary between the TiO_2 film and the electrolyte, the purple dotted line demonstrates the boundary between the diffusion layer and the bulk solution. The black orthogonal coordinate system is used to show the concentration distribution of I_3^- and I^- ions, respectively. The *x* and *y* axis demonstrate the concentration of the redox couple and distance to the junction between TCO and theTiO_2 film, respectively. The *x* axis is horizontal and the *y* axis is vertical. The positive direction of *x* and *y* axis is right and down, respectively. The green and red dotted lines are the bulk concentration of I_3^- and I^- ions, respectively. The green and red dashed lines are the concentration distribution of I_3^- and I^- ions vs. the distance, respectively.

The concentration distribution of I^- and I_3^- ions in the conventional DSC configuration as shown in Figure S1 is in favor of the charge recombination reaction while against the dye regeneration reaction, which enlightened us to develop a circulating electrolyte configuration for high performance carbon-based DSC. Reactions (1) to (6) are the reactions that take place under solar illumination, with reactions (3), (4), and (5) being the three energy-wasting recombination pathways. Dyes adsorbed on the TiO_2 film get excited and inject electrons into the conduction band of the TiO_2 with an injection rate of 10^{10} ~10^{12} s^{-1} (reaction 1); electrons in the TiO_2 film (i.e., e^-_{TiO2}) are then transported in the TCO with a transportation rate of 10^0 ~10^3 s^{-1} (reaction 2); the photo-excited dyes then become dye^+ and regenerated to neutral state by I^- ions in the TiO_2 film with a reduction rate of 10^6 ~10^8 s^{-1} (reaction 6); dye^+ ions may also get the electrons from the TiO_2 film (i.e., e^-_{TiO2}) with a charge recombination rate of 10^3~10^6 s^{-1} (reaction 3); I_3^- ions in the TiO_2 film may get the electrons from TCO (i.e., e^-_{TCO}) with a charge recombination rate of 10^0 ~10^3 s^{-1} (reaction 4 and 5, respectively).

Experimental

1) Fabrication of counter electrode (CE)

The main difference between the normal DSCs and the circulating electrolyte DSC is the CE. The CE was chosen as the electrode to insert two stainless steel pipes because it is easier to manufacture than the WE. As shown in Figure S2A, The CE consisted of a graphite electrode with two pipes on both sides. The dimension of the CE is 20 mm (length) × 20 mm (width) × 5 mm (height). The pipes on both sides are hypodermic needle made of stainless steel with an inner diameter of 0.69 mm, an outer diameter of 1.07 mm, and a length of 35 mm. The graphite block was manually polished with 1.0, 0.3, and 0.05 micro Gamma-Alpha alumina powder in a sequence to a mirror finish, and the surface was then immersed in 3M HCl, acetone, methanol and distilled water in an ultrasonic cleaner for 20 minutes, respectively, to remove any surface impurities. Afterwards, the RGO/Cu_2S was coated on the graphite electrode. The RGO/Cu_2S was prepared according to literature.[1] Then two holes with a diameter of 1.1 mm and a length of 7.5 mm were drilled on both sides of the CE. The center of the circle is located at 2 mm below the upper surface of the graphite electrode. A notch with a height of 0.35 mm and a width of 0.5 mm was cut on one side of the needles to make sure the electrolyte can be transferred into or outside the chamber between the WE and CE (Figure S2a). Next, two notches with a length of 6 mm, a width of 0.5 mm, and a height of 1.8 mm were drilled on the upper surface of the graphite electrode. The notches on the surface of graphite electrode were located in the middle of the surface with a distance of 5 mm between these two notches, as illustrated in Figure S3. These two notches on the surface were corresponding to the two notches on the needles and were also used for the electrolyte to be transported into or outside the chamber. After all these preparations, the two needles were inserted into the graphite electrode and fixed by pre-pasted quick-drying glue on the surface of the hole. The graphite electrode was then placed in a fume hood for 24 h to dry out the glue. Graphite was chosen because it has an excellent electrical conductivity (Resistivity: 2.5~5.0×10^{-6} Ω·m) and good machinability which enables the easy insertion of the stainless steel pipes.

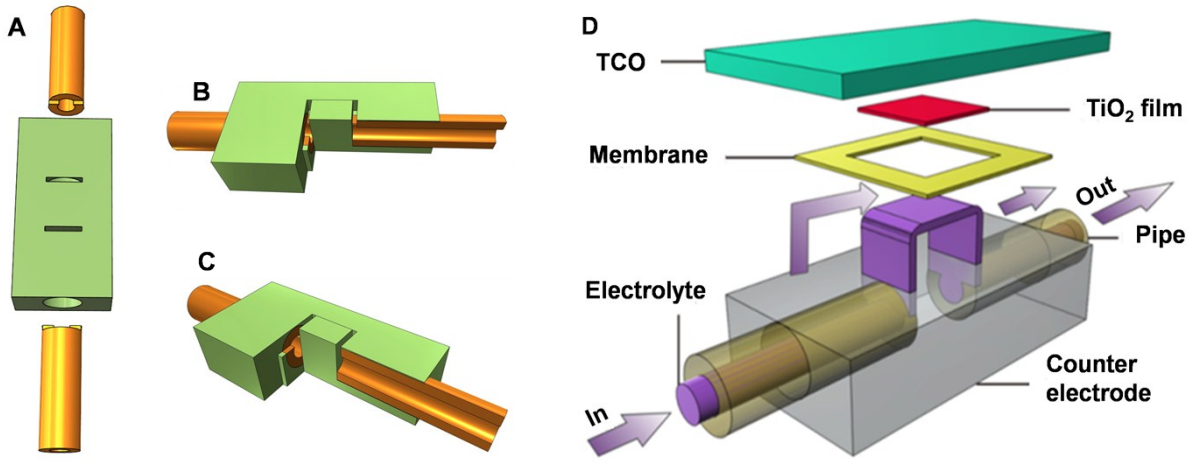

Figure S2. (A) Parts assembly drawing of the CE: the main body is made of graphite and the two pipes are made of stainless steel, (B) and (C) parts sectional views of the CE with two pipes on both sides, the notch on the needle corresponds to the notch on the graphite electrode, and (D) schematic illustration for the circulating electrolyte DSC.

2) Fabrication of working electrode (WE) and configuration of DSC

The TiO_2 paste in the WE was prepared according to a previous report.[2] Typically, a TiO_2 film was loaded on a FTO glass using a screen printing method with dense transparent TiO_2 nanoparticles of 18 nm in diameter. The TiO_2 film has a thickness of around 30 μm and a surface area of 0.25 cm^2. The TiO_2 coated FTO substrate was then sintered at 500 ºC for 1h and cooled to 100 ºC to generate the anatase nanocrystals. After that, the TiO_2 electrode was immersed in 40 mM $TiCl_4$ aqueous solution at 70 ºC for 30 min. The TiO_2 film was then annealed under N_2 at 450 ºC for 30 min. Next, the TiO_2 electrode was placed in a mixture solution of tert-butyl alcohol and acetonitrile (1:1 in volume ratio) containing 2×10^{-4} M N749 dye for 24 h. The WE was then connected to the CE by a hot-press machine with a 40 μm thick Surlyn film (DuoPont) situated in the between at 110 ºC for 1 min. The whole packing process was done in a glove box. The electrolyte solution was composed of 0.6 M dimethyl propyl imidazolium iodide, 0.1 M lithium iodide, 0.05 M iodine, and 0.5 M tert-butylpryidine in acetonitrile solution. One end of the silicone tube was connected to the pipe and the other end was inserted into the electrolyte solution to inject electrolyte into the cell. After the cell was filled with the electrolyte, the end of the silicone tube that immersed in the electrolyte solution was taken out and connected to the other pipe. In this way, the electrolyte solution could be forced to circulate in the system by a pump. The relationship between the rotating speed of the pump and the flow rate of the electrolyte was examined.

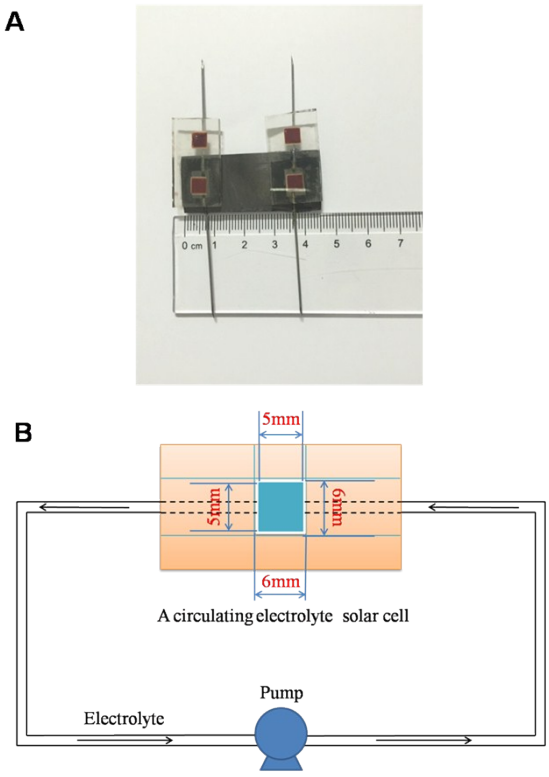

Figure S3. (A) A photograph of the circulating electrolyte DSCs, (B) The schematic diagram of the circulating electrolyte DSC system, which was composed of a circulating electrolyte DSC, a pump and a silicone tube to connect the two pipes. The size of the TiO_2 electrode was 5×5 mm, and the inner size of the Surlyn film frame was 6×6 mm.

3) Relationship between the flow rate of the electrolyte and the rotating speeds of the pump

It was found that the flow rate of the electrolyte has a nearly linear relationship with the rotating speeds of the pump, as shown in Figure S4.

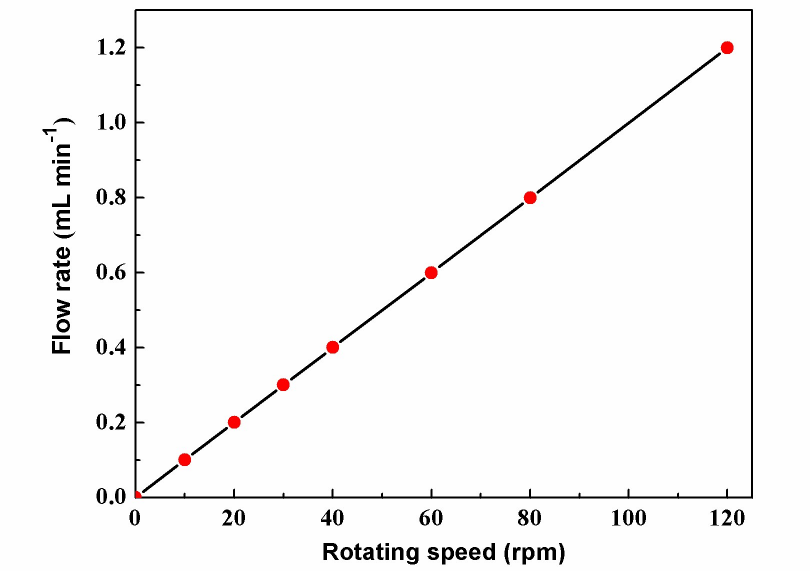

Figure S4. A relationship between the rotating speeds of the pump and the flow rates of the electrolyte.

4) Photovoltaic characterization

The photovoltaic measurements were carried out in a device with a UV- cut-off filter and masked with a thin metal mask to give an active area of 0.25 cm^2. *J-V* curves of the circulating electrolyte DSC were measured with a digital source meter (Keithley 2400) under simulated solar illumination at 100 mW cm^{-2}, AM 1.5 G standard (Wacom, Japan). The excitation beam coming from a 300 W xenon lamp (ILC Technology, USA) was focused through a Gemini-180 double monochromator (JobinYvon Ltd., UK) and chopped at approximately 4 Hz. A black metal mask was used with an aperture area of 0.25 cm^{-2} during *J-V* measurements. The effect of the mass transfer mechanism of electrolyte on the efficiency of the circulating electrolyte DSC was investigated by changing the rotating speed of the pump from 0 to 120 rpm (0, 10, 40, 80, and 120 rpm, respectively). Dark current density-voltage curves were measured with the circulating electrolyte DSC in dark. For the open-circuit voltage decay (OCVD) measurements, the circulating electrolyte DSC was illuminated to a steady voltage, then the illumination was turned off with a shutter, placing neutral density filters in the illumination path performed a systematic change of the initial steady-state conditions. The OCVD was recorded by an Ecochemie potentiostat equipped with a short-interval sampling module as has been reported in literature.[3]

To measure the diffusion coefficient and the mass transfer coefficient of the redox couple, chronoamperometry method and the relationship between the mass-transfer limited current and mass-transfer coefficient were used, respectively. A traditional three electrode system was used for the electrochemical measurements. All the electrochemical experiments were carried out with an electrochemical workstation (Zahner IM6, Germany). The WE was a microelectrode with a radius of 5 μm, a Pt sheet electrode with an apparent area of 4 cm^2 was used as the CE, and a home-made reference

electrode that consisted of a silver wire immersed in 10 mM $AgCF_3SO_3$/ Acetonitrile separated from the bulk solution by porous glass as reported previously was used.[4] The WE and CE electrodes were dipped in an anhydrous acetonitrile solution containing 0.1 mM $LiClO_4$, 10 mM LiI, and 5 mM I_2. To measure the mass-transfer limited current in the traditional three electrode system, a rotor was put into the electrolyte cell, and the electrolyte solution was stirred at different rates (i.e., 100, 200, and 400 rpm, respectively). UV-vis absorption spectra were recorded using a Hitachi U-4100 (Japan) spectrophotometer.

Results

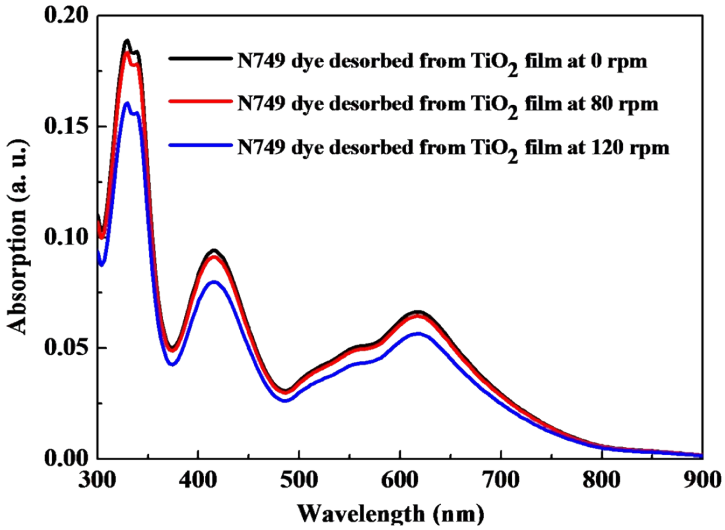

Figure S5. UV-vis absorption spectra of the desorbed dye from TiO_2 film used after the *J-V* measurements.

It can be seen that the dye amounts after the *J-V* curves measurements at 0 rpm and 80 rpm were almost the same, while the dye amount on the TiO_2 film after the *J-V* curve measurement at 120 rpm was much less, which means that at a relatively high flow rate (i.e., larger than 80 rpm), dyes may be washed away from the TiO_2 film. This may be the main reason for the smaller V_{oc}, J_{sc}, *FF* and η observed at 120 rpm than the values obtained at 80 rpm. The power conversion efficiency slightly decreases in the range between 80-120 rpm owing to the extremely fast flow rate of the electrolyte which washed away the adsorbed dyes.

Table S1. The power (P) and power conversion efficiency (η) of the circulating electrolyte DSC at various rotating speeds.

Speed (rpm)	P_f (mW)	P_{max} (mW)	P (mW)	η (%)
0	0	1.727	1.727	6.91
10	$2.337*10^{-3}$	2.065	2.063	8.25
40	$3.739*10^{-2}$	2.543	2.506	10.02
80	0.1496	2.722	2.573	10.29

P_f stands for the power consumed by the pressure drop resulted from the electrolyte flowing through the cell, P_{max} stands for the maximum power of the circulating electrolyte DSC, and P stands for the overall power of the circulating electrolyte DSC.

Table S1 shows the power and power conversion efficiency of the circulating electrolyte DSCs at various rotating speeds after subtraction of the energy consumed by the pump. The energy consumed by circulating the electrolyte through the pump was estimated by only considering the pressure drop resulted from the friction in the cell. Evidently, compared with the overall efficiencies without subtraction of the energy consumed, the subtracted efficiencies due to the energy consumed by the pump are fairly low, even at a high rotating speed (e.g., ca. 5.83% of the overall efficiency at 80 rpm), and as a result, the net power conversion efficiency (i.e., after subtraction of the energy consumed) is still very impressive (i.e., 10.29%), much higher than the efficiency of DSC with the stationary electrolyte case (i.e., 6.91%).

There are other methods to circulate the electrolyte without using a pump, and one of them is utilizing the temperature-sensitive magnetic fluid (TSMF). TSMF is an effective medium capable of transporting mass heat for small temperature differences.[5-7] Similar experiments were also done in our study by adding the TSMF into the electrolyte solution as described by literature,[5,6] and the flow resulted maximum velocity of the electrolyte without using a pump was about 20 mm/s, which is equivalent to a flow rate of 10 rpm using the pump. The results demonstrate that the TSMF is also a promising method to circulate the electrolyte to enhance the performance of the DSCs.

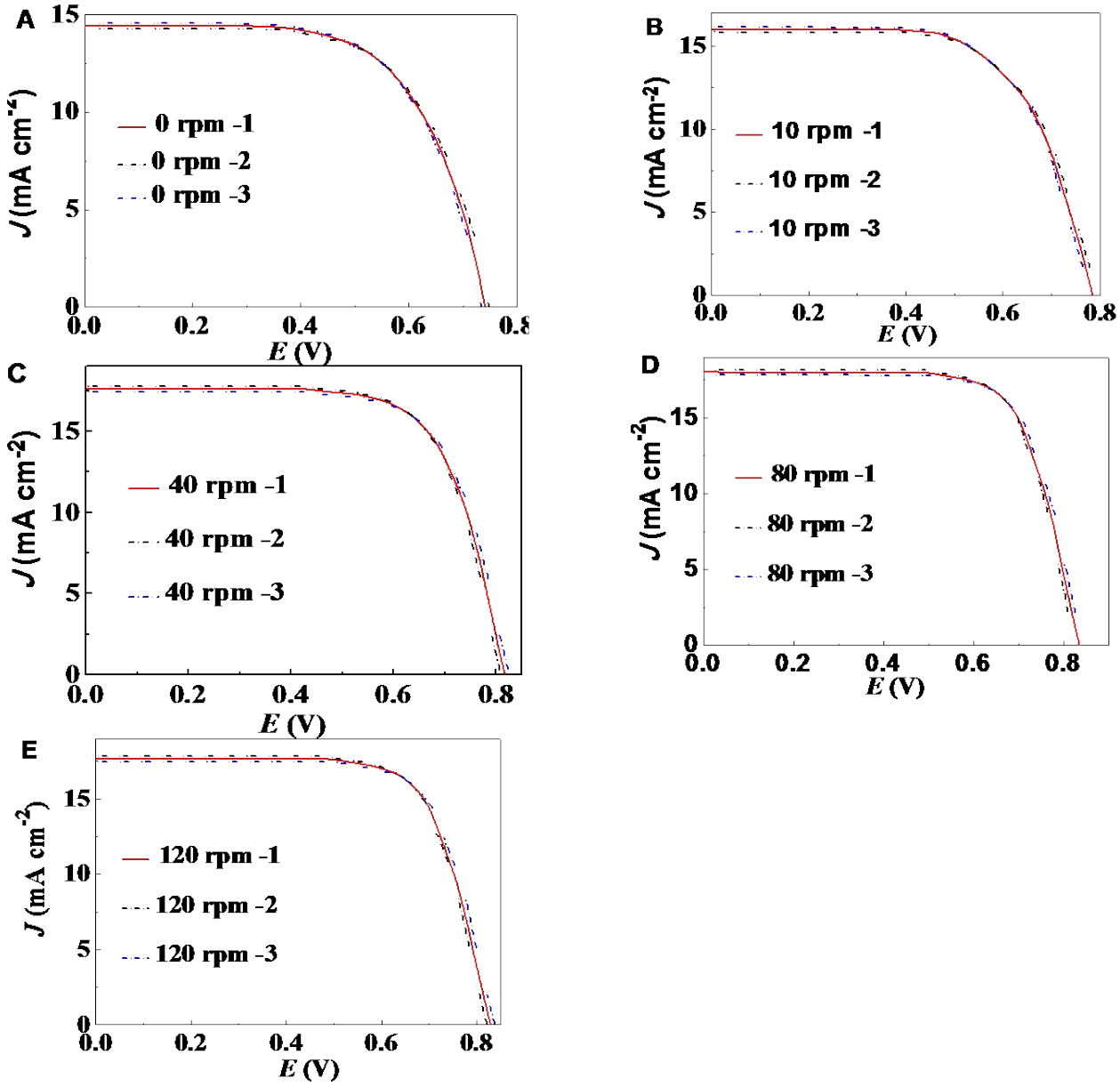

Figure S6. Repeated *J-V* characteristics of the circulating electrolyte DSCs. The DSCs were prepared at the same condition and measured under AM 1.5 illumination, the active area of all DSCs is 0.25 cm², rotating speeds: (A) 0 rpm, (B) 10 rpm, (C) 40 rpm, (D) 80 rpm, and (E) 120 rpm.

Table S2. Representative photovoltaic parameters for the DSCs with Pt-free CEs.

CE	V_{oc} (V)	J_{sc} (mA cm^{-2})	*FF* (%)	η	Reference
Pt	0.72	15.95	0.70	7.79	26
HCMSC	0.74	15.81	0.67	7.56	26
CMK-3	0.73	15.65	0.61	7.03	26
AC	0.73	15.00	0.54	6.24	26
OMPC	0.75	16.86	0.69	8.67	28
Core–shell NDG/CoS	0.71	20.38	0.74	10.71	24
Ti/TiC	0.78	13.12	0.70	7.15	23
VC-Mo_2C	0.81	13.11	0.72	7.63	22
Graphite-S	0.74	14.45	0.65	6.91	This study
Graphite-C	0.84	17.99	0.73	10.29	This study

Notes: HCMSC: hollow core/mesoporous shell carbon, CMK-3: ordered mesoporous carbon, AC: activated carbon, OMPC: Ordered multimodal porous carbon, NDG: N-doped graphene, Graphite-S: graphite CE combined with a stationary electrolyte, Graphite-C: graphite CE combined with a circulating electrolyte after subtraction of the energy consumed.

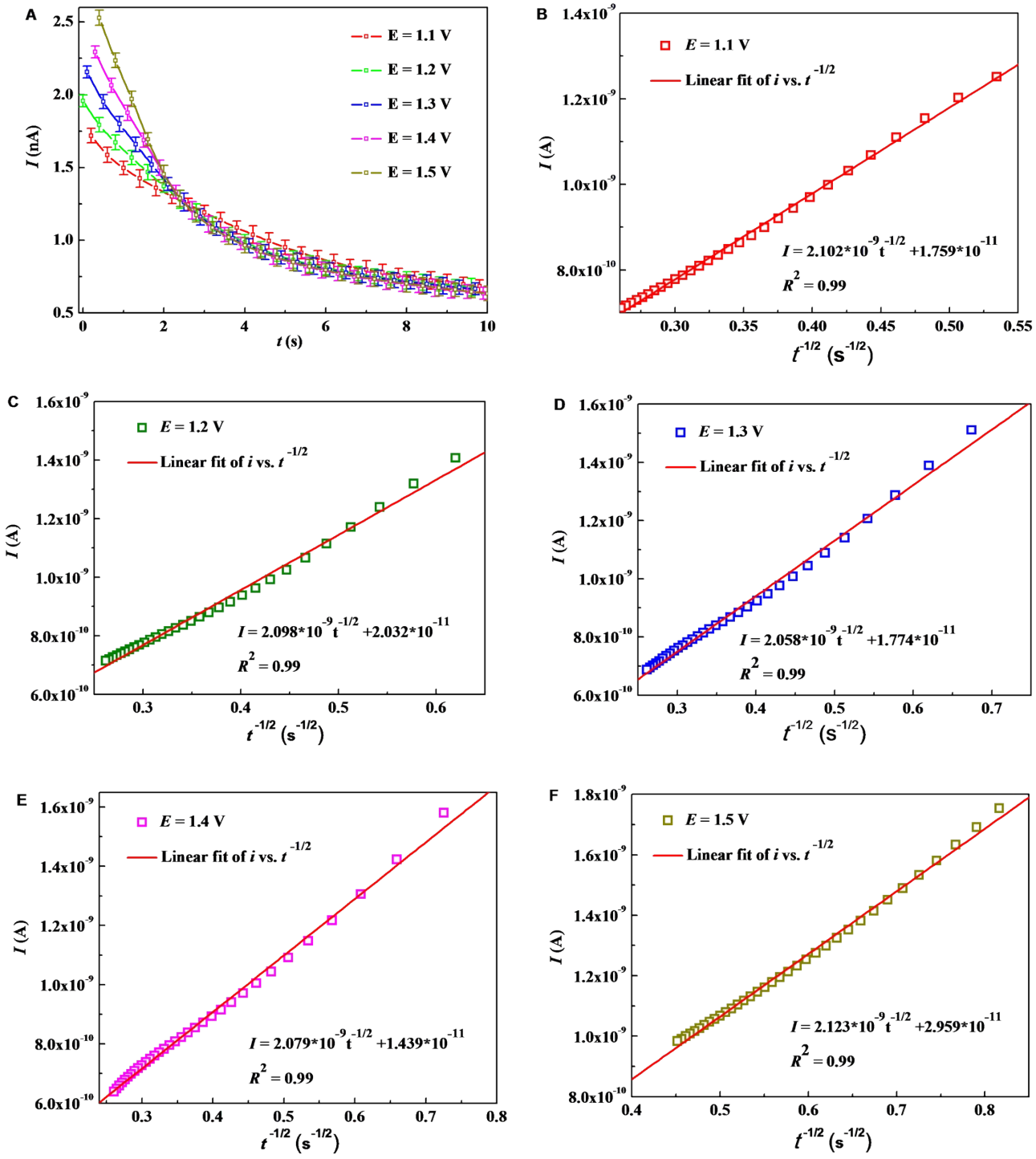

Figure S7. Original data with error bars and the linear fit of i vs. $t^{-1/2}$ plots: (A) chronoamperometric curves of I_3^- ions with error bars. (B), (C), (D), (E), and (F) linear fit i vs. $t^{-1/2}$ at different step potentials and the fitting results, E = 1.1 V, 1.2 V, 1.3 V, 1.4 V, and 1.5 V, respectively.

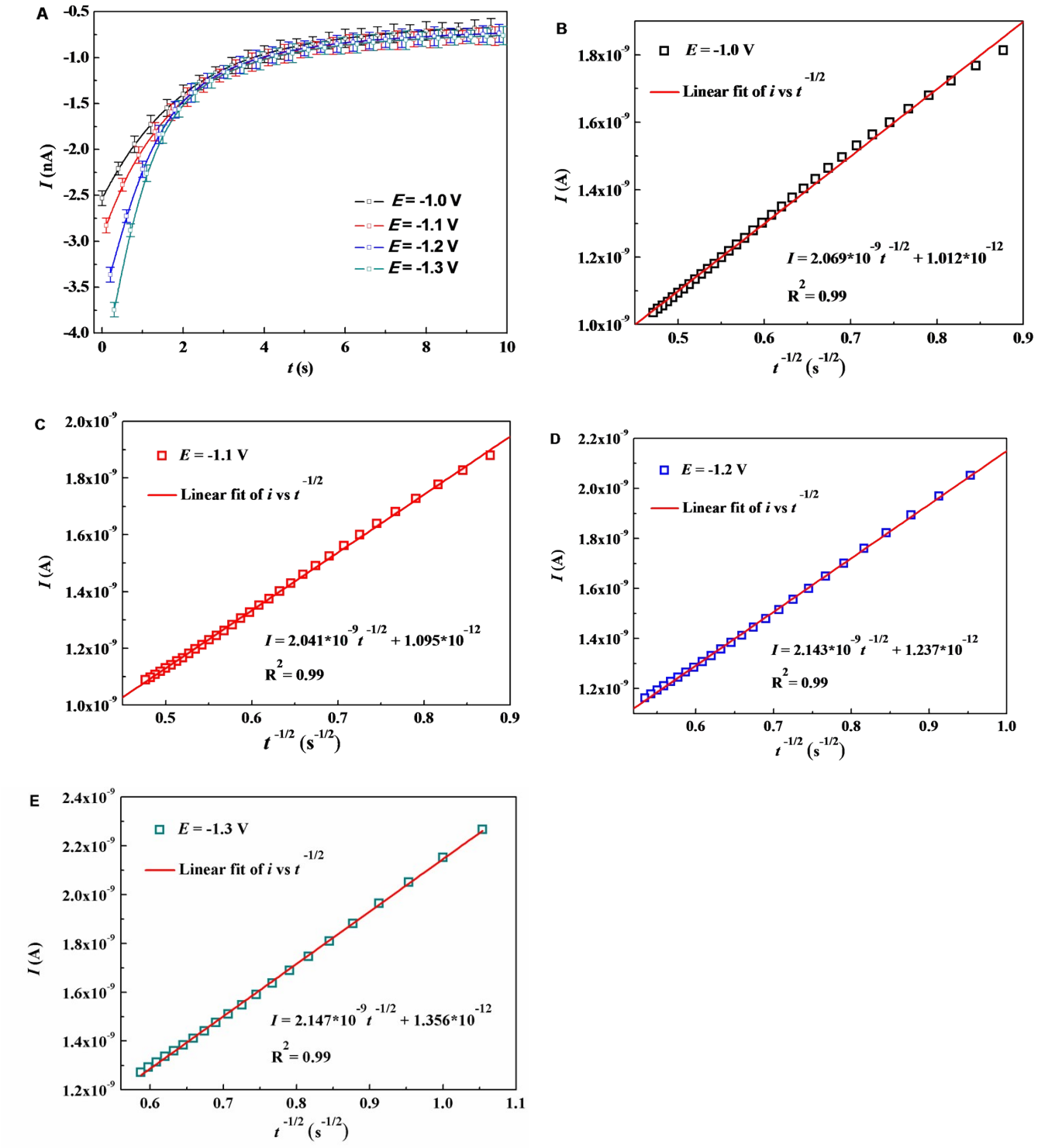

Figure S8. Original data with error bars and the linear fit of i vs. $t^{-1/2}$ plots. (A) chronoamperometric curves of I^- ions with error bars. (B), (C), (D), and (E) linear fit i vs. $t^{-1/2}$ at different step potentials and the fitting results, E = -1.0 V, -1.1 V, -1.2 V, and -1.3 V, respectively.

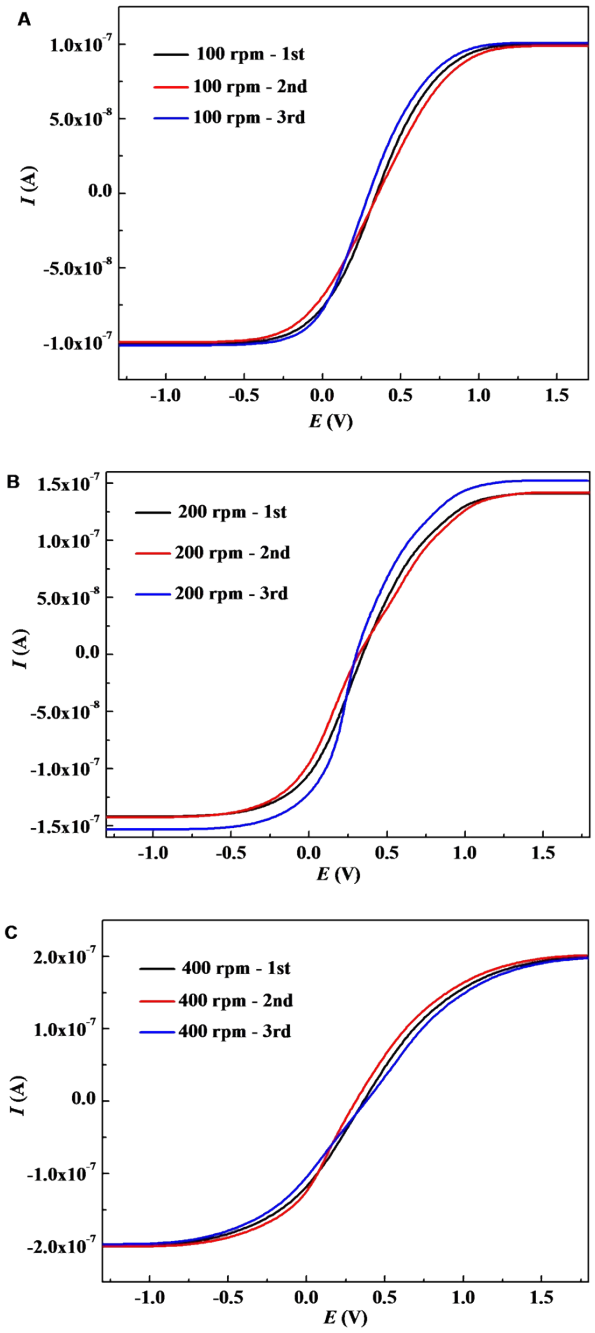

Figure S9. Mass-transfer limiting current of I^- and I_3^- ions vs. *E* at different stirring rates (100, 200, and 400 rpm) measured at the same condition.

References

1 E. Bi, Y. Su, H. Chen, X. Yang, M. Yin, F. Ye, Z. Li and L. Han *RSC Adv*. 2015, ***5***, 9075.

2 C. Qin, A. Islam and L. Han, *Dyes and Pigments,* 2012, **94**, 553.

3 A. Zaban, M. Greenshtein and J. Bisquert, *ChemPhysChem*, 2003, **4**, 859.

4 S. Gu, X. Wang, Y. Wei and B. Fang, *Nucl. Sci. Tech.* 2015, **26**, S10307.

5 K. Fumoto, H. Yamagishi, M. Ikegawa, M. *Nanoscale and microscale thermophysical engineering*, 2007, **11**, 201-210.

6 T. Fujita, T. Miyazaki, H. Nishiyama, *Journal of magnetism and magnetic materials*, 1999, **201**, 14-17.

7 Y. Iwamoto, K. Takeda, X. Niu, et al. *Journal of the Japanese Society for Experimental Mechanics*, 2013, **13** (Special Issue): s18-s23.